Journal of the American Society for Mass Spectrometry

pubs.acs.org/jasms Article

Top-Down Electron Detachment Dissociation at ∼15−92 eV and 9.4 T with High Space Charge Capacity FT-ICR Cells

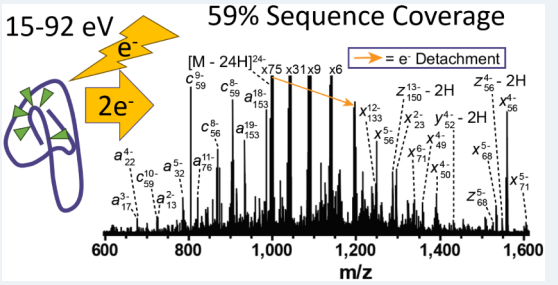
Published as part of Journal of the American Society for Mass Spectrometry special issue "Advances in Fourier Transform Mass Spectrometry".

Steven A. DeFiglia, Nathan K. Kaiser, Greg T. Blakney, Marek Polák, and Kristina Håkansson*

Cite This: https://doi.org/10.1021/jasms.6c00260 Read Online

ACCESS | Metrics & More | Article Recommendations | Supporting Information

ABSTRACT: Top-down mass spectrometry (TD-MS) allows detailed characterization of biomolecular heterogeneity, e.g., sequence variants, chemical and biological modifications, and mutations. While relatively established in positive-ion mode, negative-ion-mode TD-MS of intact proteins has been less explored, in part due to a lack of suitable activation approaches for tandem mass spectrometry. Here, we show that electron detachment dissociation (EDD) can yield analytically useful sequence coverage up to ∼60% for β-casein (24 kDa), with relatively straightforward spectral interpretation due to favored formation of *a*• and *x*-type fragments with limited neutral loss. This leap in EDD performance from previously reported 5% sequence coverage was enabled by use of a custom wide-bore 9.4 T FT-ICR instrument with a solid dispenser cathode for optimal anion-electron overlap. In addition, a prototype—now commercially available—instrument with a dynamically harmonized ICR cell and a hollow cathode yielded 51% sequence coverage for β-casein, more than an order of magnitude higher than previous reports. EDD of phosphorylated α- and β-casein proteins showed phosphate retention in fragment ions and allowed phosphorylation site determination. High-energy, ∼72−92 eV, EDD is demonstrated to enable shorter irradiation times than previously reported, as low as 3 ms for an RNA 18-mer (100% sequence coverage) and 35 ms for carbonic anhydrase (47% sequence coverage), although higher electron energy results in lower average fragment ion charge. Numerous (*y* − 2H) fragments from backbone cleavage near proline were observed, indicative of electronic excitation under EDD conditions. Electron energy vs irradiation time heatmaps provide an in-depth understanding of how to tune EDD for desired fragmentation outcomes. Overall, the presented results show promise for incorporating EDD in online liquid chromatography-TD-MS workflows.



INTRODUCTION

Protein and RNA sequence information, including sites of chemical or post-translational modification (PTM), can be obtained by tandem mass spectrometry (MS/MS). In typical bottom-up approaches[1−4] biomacromolecules are digested with enzymes such as trypsin or ribonucleases into peptides or lower molecular weight oligonucleotides, respectively, which are analyzed by liquid chromatography (LC)-MS/MS. While bottom-up analysis offers high peptide or oligonucleotide sequence coverage, including site localization of many PTMs and other modifications, information about proteoform or RNA heterogeneity, i.e., what specific combinations of PTMs, chemical modifications, sequence variants, and truncations are present is lost upon digestion.[4−6] Top-down analysis (TD-MS)[6−10] of undigested biomolecules provides a more accurate depiction of this heterogeneity; however, sequence coverage is often limited in TD-MS due to a lack of large fragment ions from backbone cleavage in the central portion of biomolecules.

Protein TD-MS is typically performed with positive ion mode electrospray ionization (ESI). A number of MS/MS activation techniques have been implemented to maximize sequence coverage, including both beam- and resonance-type collision-induced dissociation (CID), electron capture dissociation (ECD), electron transfer dissociation, and ultraviolet photodissociation (UVPD).[11−14] However, the average isoelectric point of the human proteome is estimated to be ∼6.7,[15] which indicates that many proteins should preferentially ionize in negative rather than positive ion mode ESI. Additionally, acidic PTMs, e.g., phosphorylation, sulfation and sialylation, which regulate protein function, are common in

Received: July 4, 2026
Revised: September 16, 2026
Accepted: October 6, 2026

ACS Publications © XXXX The Authors. Published by American Chemical Society

Downloaded from pubs.acs.org/jamsse/article-pdf/doi/10.1021/jasms.6c00260/6901816/jasms.6c00260.pdf by FLORIDA STATE UNIV user on 02 November 2026

eukaryotic cells.[16−20] Such acidic PTMs can further reduce positive mode ionization efficiency. Negative ion mode is also the preferred polarity for RNA and DNA analysis due to the facile deprotonation of the phosphodiester backbone.[9,21−23]

While negative ion mode TD-MS is emerging as an analytical strategy for nucleic acids, in part due to improvements in MS instrumentation,[9,23−25] protein anion TD-MS has seen limited implementation,[26−28] mainly due to a lack of suitable MS/MS activation techniques. Widely available slow heating activation methods, such as CID, and infrared multiphoton dissociation (IRMPD) yield complex fragmentation patterns, including a variety of backbone and side chain bond cleavages in negative ion mode.[27] Recent work by Brodbelt and coworkers demonstrated that UVPD offers high sequence coverage in negative ion mode protein TD-MS.[26] However, UVPD can suffer from high false discovery rate due to generation of all possible fragment ion types, i.e., *a*/*b*/*c*/*x*/*y*/*z* ions, as well as neutral losses and internal fragments.[29,30] Electron-based MS/MS techniques[31] have also been employed for negative ion mode TD-MS. Negative ion electron capture dissociation (niECD) was demonstrated to yield a charge-increased species following irradiation of MALDI-generated singly deprotonated ubiquitin with ∼6 eV electrons, however no fragment ions were detected and thus niECD, at this time, does not appear suitable for TD-MS.[32] Negative electron transfer dissociation (NETD) is still under development for TD-MS and not yet commercially available. Recent work reported improved sequence coverage with the use of xenon gas, a limited resource, for generating reagent cations.[33] Further IR activation has also been shown to be required to liberate fragment ions, or to unfold the precursor ion during electron transfer for improved fragment ion detection.[33,34]

Electron detachment dissociation (EDD)[35] involves irradiation of polyanions with ≥10 eV electrons, resulting in electron ejection and radical-driven fragmentation, which has shown promise for nucleic acid TD-MS.[9,22,23,36] By contrast, previous protein TD-MS with EDD showed limited sequence coverage; 19% for an acidic ∼16 kDa protein[28] and only 5% for multiply phosphorylated, ∼24 kDa β-casein.[27] Abundant CO_2 neutral losses further diluted sequence-informative fragment ion signal and thus may limit analytical utility. However, previous publications on protein top-down EDD used 7 T Bruker Apex-Q Fourier transform ion cyclotron resonance (FT-ICR) instruments equipped with Infinity trapped ion cells[37] and hollow cathodes[38] for electron generation/injection (Figure S1). This type of ICR cell has limited space charge capacity, which is easily exceeded when injecting a high number of electrons into a polyanion cloud. Consequently, EDD performance in this geometry was found to be highly sensitive to the voltage on an electron extraction lens located between the hollow cathode and the ICR cell; a negative potential close to the cathode bias voltage was required to limit the number of electrons entering the ICR cell.[39,40] Furthermore, precursor anion-electron overlap for high efficiency EDD can be challenging in this geometry.[39,40] This ion cloud-electron beam overlap issue in off-axis implementations such as the hollow cathode is well documented for more efficient cation-electron reactions with supplemental sustained off-resonance irradiation allowing for ion cloud position manipulation during electron irradiation for improved fragmentation outcomes.[41]

Here, we present top-down EDD on two higher magnetic field instruments (9.4 T), built by Alan Marshall's research group[42,43] and commercially available from Bruker,[44] respectively. The new generation Bruker FT-ICR instruments are equipped with larger volume, higher space charge capacity dynamically harmonized trapped ion cells[45,46] whereas a previously built, large volume electrically compensated cell[47,48] was used in the custom instrument. Space charge capacity is further improved compared with previous experiments due to the increase in magnetic field strength. Marshall and Guan showed that the maximum number of charges in an ICR cell increases as the square of the magnetic field,[49] i.e., an increase from 7 to 9.4 T should improve space charge capacity by a factor of 1.8. The custom instrument is also equipped with a solid surface dispenser cathode for improved ion-electron overlap.[50−52] Optimization of EDD conditions in these instruments demonstrated efficient fragmentation of both proteins up to ∼30 kDa and an 18-mer RNA with irradiation times as low as 3 ms, shorter than what has been demonstrated with alternative EDD-compatible instrumentation such as the chimera cell[36,53] and Omnitrap platforms.[23]

MATERIALS AND METHODS

Sample Preparation

Bovine ubiquitin (∼8.6 kDa), bovine α-S1-casein (∼24 kDa), bovine β-casein (∼24 kDa), bovine erythrocytes carbonic anhydrase II (CAII, ∼29 kDa), baker's yeast enolase (∼47 kDa), bovine apocalmodulin, (∼16.7 kDa) triethylamine (TEA), 1,5-diazabicyclo[4.3.0]non-5-ene (DBN), piperidine (PIP), and Amicon 3 kDa spin filters were all purchased from Sigma-Aldrich (St. Louis, MO, USA). Unmodified, HPLC-grade Nusinersen oligonucleotide (5′OH-UCA CUU UCA UAA UGC UGG-3′OH) was purchased from GenScript (Piscataway, NJ, USA). LC-MS grade water and methanol were purchased from Honeywell Burdick & Jackson (Charlotte, NC, USA). Protein samples were desalted with 3 kDa Amicon spin filters following the manufacturer's protocol, then prepared into 1:1 methanol:water with 0.1% TEA, DBN, or PIP basic additives to a concentration of ∼1−5 μM. Nusinersen was dissolved in 1:1 methanol:water with 1% PIP to a final concentration of 16 μM.

Fourier Transform Ion Cyclotron Resonance Mass Spectrometry

Samples were directly infused with ESI at up to 3 μL/min with a 1.1−3 kV high voltage, applied to a stainless steel union, through a 50 μM I.D. tapered fused silica emitter into the heated metal capillary of a passively shielded, 220 mm bore, home-built 9.4 T FT-ICR mass spectrometer equipped with an open, seven-segment electrically compensated ICR cell[47,48] (Figure S1). Samples were also infused at the same flow rate into a prototype Bruker trapped ion mobility spectrometry (TIMS)-FT-ICR (timsMRMS) instrument[44] with a dynamically harmonized cell[45,46,54] (Figure S1) in an actively shielded 9.4 T magnet. Ions in both instruments were quadrupole isolated at a width of 10 *m*/*z* and externally accumulated[55] for up to 5 s. Ions were then transferred to the ICR cell, where they were confined by either −3 or −4 V trapping voltages on the outermost cell electrodes or trapping plates. Stored waveform inverse Fourier transform (SWIFT)[56,57] was employed for in-cell precursor ion isolation in the custom 9.4 T instrument.

Electron Detachment Dissociation

The custom wide bore FT-ICR instrument is equipped with a 1.016 cm diameter solid cathode (HeatWave, Watsonville, CA) (Figure S1) mounted 73 cm from the axial center of the ICR cell. The cathode was conditioned with a 3.5 A heating current and operated at 3.2 A. For reproducible electron flux, the cathode was routinely warmed overnight before each experiment and left on for the duration of the experiments. A molybdenum grid, used to control electron flux, was located in between the cathode and the ICR cell at a distance of 8 mm from the cathode. EDD was performed for 1−800 ms at cathode bias voltages of −20 to −100 V with the molybdenum electron extraction

Downloaded from pubs.acs.org/jamsef/article-pdf/doi/10.1021/jasms.6c00260/6901816/jasms.6c00260.pdf by FLORIDA STATE UNIV user on 02 November 2026

https://doi.org/10.1021/jasms.6c00260
J. Am. Soc. Mass Spectrom. XXXX, XXX, XXX−XXX

grid voltage set to positive 2−5 V relative to the cathode bias voltage. Following electron irradiation, a 100 ms electron cleanup event was performed to reduce space charge prior to anion excitation. The relationship between cathode bias voltage and electron energy was established by measuring the current on a transfer quadrupole on the opposite side of the ICR cell as a function of a repelling voltage at a 5 V offset between the cathode and electron extraction grid, as illustrated in Figure 1 and Figure S2. The prototype Bruker platform

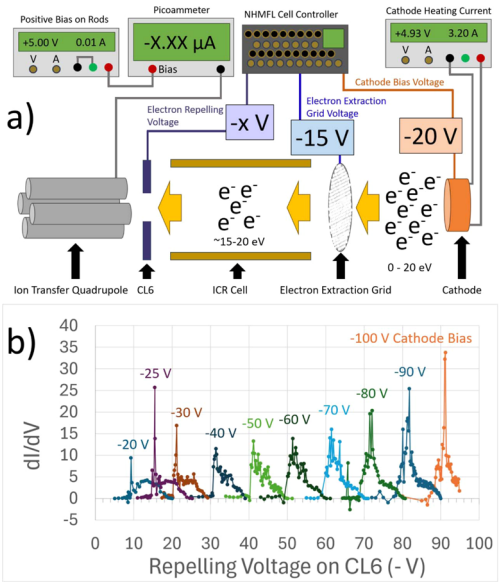


Figure 1. a) Electron energy measurements and set up. Electrons were measured on the positively biased quadrupole rods with a Keithley 485 picoammeter. Electrons were generated by a solid cathode (Heatwave, Watsonville, CA), indirectly heated at 3.20 A. Electron energy was altered by changing the cathode bias voltage, whereas electron flux was controlled with a +5 V offset on the electron extraction grid relative to the cathode bias voltage. Numbers shown are for a −20 cathode bias voltage. b) Measured current on the quadrupole rods at various cathode bias voltages upon application of an increasingly negative, electron repelling potential on conductance limit 6 (CL6, Figure 1a).

was outfitted with a hollow cathode (Figure S1), conditioned to 1.5 A and operated at 1.5 A. EDD experiments with the Bruker timsMRMS instrument were performed with a 130 ms irradiation time, −30 cathode bias voltage, and −20 electron extraction lens voltage. For each EDD experiment on either instrument, 800−3200 ms transients were acquired.

Data Analysis

EDD data were processed with either PredAnalysisCore v6.1.2.7 or Bruker DataAnalysis version 6.2. Spectra were internally recalibrated using high confidence fragment ions, then manually annotated with Predator Manual Validation v.2.9.1 and Protein Prospector, or Mongo Oligo mass calculator v2.07. Because many fragment ions show low signal-to-noise (S/N) ratios ±5 ppm mass accuracy was accepted. To account for mismatches between deprotonation state and fragment ion charge due to electron detachment, up to three hydrogen atom losses were assigned. Protein and oligonucleotide sequence coverage figures were generated with a custom Python script. When the deviation between calculated and observed isotopic distributions indicated more than one hydrogen loss, assignments were included in a separate color. For ubiquitin, the average fragment ion charge states from different EDD conditions were calculated based on annotated *a*- and *x*-type ions.

RESULTS AND DISCUSSION

High Space Charge Capacity EDD of Casein Phosphoproteins

Our initial experiments focused on *β*-casein, which was previously shown to yield only 5% sequence coverage from EDD. We first replicated the previous approach which did not involve any protein desalting or quadrupole isolation, i.e., broadband EDD of all observed charge states (10− to 23−). With the custom FT-ICR instrument, we observed a sequence coverage of ∼30%, six times higher than previous results (Figure S3) with some optimization of the cathode bias voltage. These data allowed site localization of all five phosphoserines through N-terminal phosphate-retaining fragment ions. Such unambiguous PTM site determination, is hampered in positive-ion mode ECD, presumably due to salt bridge formation.[27,58] For example, Ge and coworkers noted a slight decrease in the number of observed fragment ions in phosphorylated forms of proteins in top-down ECD with single phosphorylation having a minimal effect. By contrast, multiple phosphorylations in close proximity, e.g., *β*-casein resulted in a significant reduction in ECD bond cleavages, causing phosphorylation site ambiguity.[58] While previous *β*-casein EDD offered only limited phosphosite characterization, negative ion mode IRMPD provided fragmentation that localized 3/5 phosphoserines.[27] However, the corresponding IRMPD spectrum was highly complex, including neutral loss of phosphoric acid, which is not observed in EDD.

Following the success of broadband EDD with the custom FT-ICR instrument, we quadrupole isolated the 24− charge state with a 10 Th wide isolation window, followed by further proteoform-specific SWIFT isolation in the ICR cell. The protein was also desalted prior to analysis. The two known *β*-casein proteoforms, A1 (H67) and A2 (P67), were both observed (Figure S4). After further optimization of the cathode bias voltage and electron irradiation time, EDD of the 24− charge state of the A2 *β*-casein proteoform at −20 V cathode bias with 700 ms irradiation time generated a rich spectrum with nearly 60% sequence coverage, as shown in Figure 2. The data represent a greater than 1 order of magnitude increase in sequence coverage compared with previous literature values.[27] In this spectrum, a high number of N-terminal *a*/*a*• and *c*′-type fragments were observed, which may be due to the high density of acidic sites, including phosphoserine and several glutamic acids, in the N-terminal portion of the protein. The lower density of acidic sites in the C-terminal portion of *β*-casein also likely explains the lower numbers and lower overall charge states of C-terminal *x*- and *z*-type fragments. Similar to previous EDD, multiple electron ejections were observed to yield abundant charge-reduced unfragmented precursor ions. Neutral loss of CO_2 from these charge-reduced precursor ions was also observed. Theoretical masses of $(z - 2H)$ vs $(x - CO_2)$ fragments differ by only 0.02 Da and were assigned according to mass accuracy (if <5 ppm error was required, these fragment ion types could not be differentiated) and residue specificity ($(z - 2H)$ fragments are favored at serine, threonine, and tyrosine).[59] Both fragment types have been observed[28,59] and provide near identical sequence information. In contrast to previous peptide EDD,[60−62] only limited neutral losses were observed in top-down EDD from structurally informative backbone fragments, which simplified annotation.

EDD of *β*-casein was also performed on a prototype Bruker timsMRMS instrument under the same conditions as the

Downloaded from pubs.acs.org/jamsef/article-pdf/doi/10.1021/jasms.6c00260/6901816/jasms.6c00260.pdf by FLORIDA STATE UNIV user on 02 November 2026

https://doi.org/10.1021/jasms.6c00260
J. Am. Soc. Mass Spectrom. XXXX, XXX, XXX−XXX

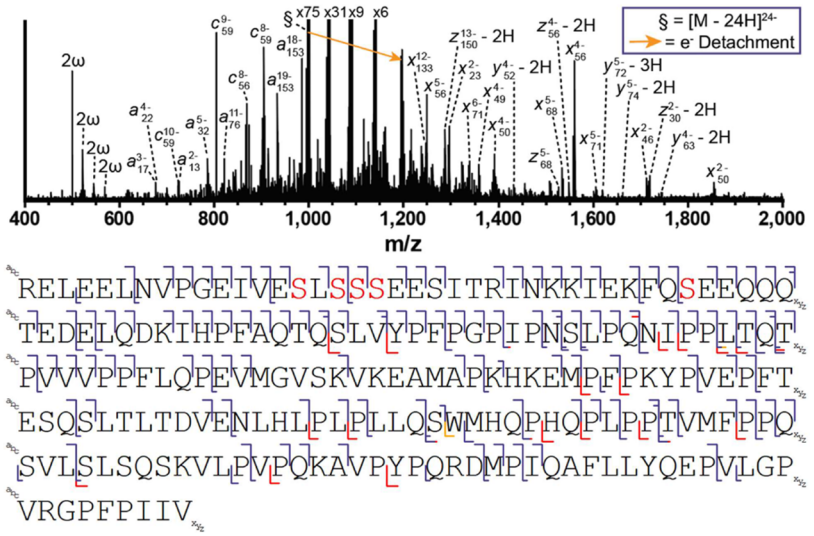


Figure 2. Top) EDD spectrum of the 24− charge state of the A2 proteoform of β-casein with a custom 9.4 T FT-ICR instrument, including some fragment ion annotations. The "§" denotes the 24− precursor ion and the "2ω" denote second harmonics. No fragment ions were observed below m/z 400. Bottom) Sequence coverage map from EDD of β-casein A2, 24− with the custom instrument, showing a sequence coverage of 59% (123/208 possible interresidue cleavages). Purple brackets represent cleavage sites for expected backbone fragment ions, red brackets represent (y − 2H) fragment ions or other fragments with ≥2 hydrogen loss, and gold brackets indicate CO_2 loss. Phosphoserine locations are indicated by red colored "S". Experimental conditions: 5 μM, 250 scans, quadrupole + SWIFT isolation, −20 cathode bias voltage −18.2 electron extraction grid voltage, 700 ms irradiation.

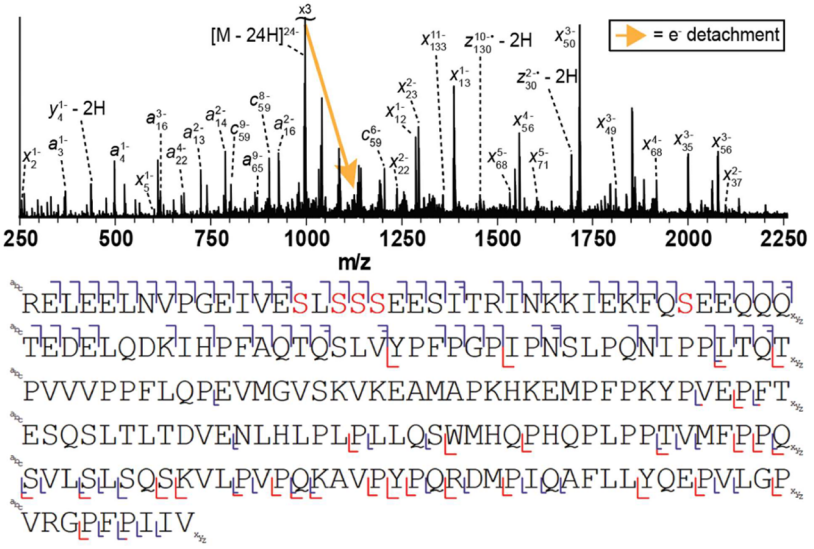


Figure 3. Top) EDD spectrum of the 24− charge state of the A2 proteoform of β-casein with a prototype 9.4 T TIMS-FT-ICR mass spectrometer, including some fragment ion annotations. Bottom) Sequence coverage map from EDD of β-casein A2, 24− with the prototype commercial instrument, showing a sequence coverage of 51% (106/208 possible interresidue cleavages). Purple brackets represent cleavage sites for expected backbone fragment ions, while red brackets represent (y − 2H) fragment ions or other fragments with ≥2 hydrogen loss. Phosphoserine locations are indicated by red colored "S". Experimental conditions: 5 μM, 250 scans, quadrupole isolation, −20 cathode bias voltage −18.5 electron extraction lens voltage, 700 ms irradiation.

custom instrument, reaching a sequence coverage of ∼51% upon fragmenting the same 24− charge state (Figure 3). While the sequence coverage at optimized conditions was lower than with the custom instrument, this result still demonstrates an order of magnitude improvement from previously published β-casein EDD performed with a commercially available platform. Furthermore, lower molecular weight fragment ions, originating from backbone bond cleavages near the protein termini, that were absent on the custom instrument were detected, providing complementary information. Both instruments generated EDD spectra with sufficient coverage of the densely phosphorylated region to allow unambiguous phosphosite determination. The observed fragment ion types were also similar, showing primarily *a*/*x*-type ions and a smaller number of *c*/*z*-type fragments.

We also performed EDD of α-casein, which is known to have up to 9 phosphorylation sites, with the most abundant proteoform bearing 8 phosphorylations. The 23− charge state of this octuply phosphorylated protein was quadrupole and SWIFT isolated and fragmented by EDD on the custom FT-

https://doi.org/10.1021/jasms.6c00260
J. Am. Soc. Mass Spectrom. XXXX, XXX, XXX−XXX

Downloaded from pubs.acs.org/jamsef/article-pdf/doi/10.1021/jasms.6c00260/6901816/jasms.6c00260.pdf by FLORIDA STATE UNIV user on 02 November 2026

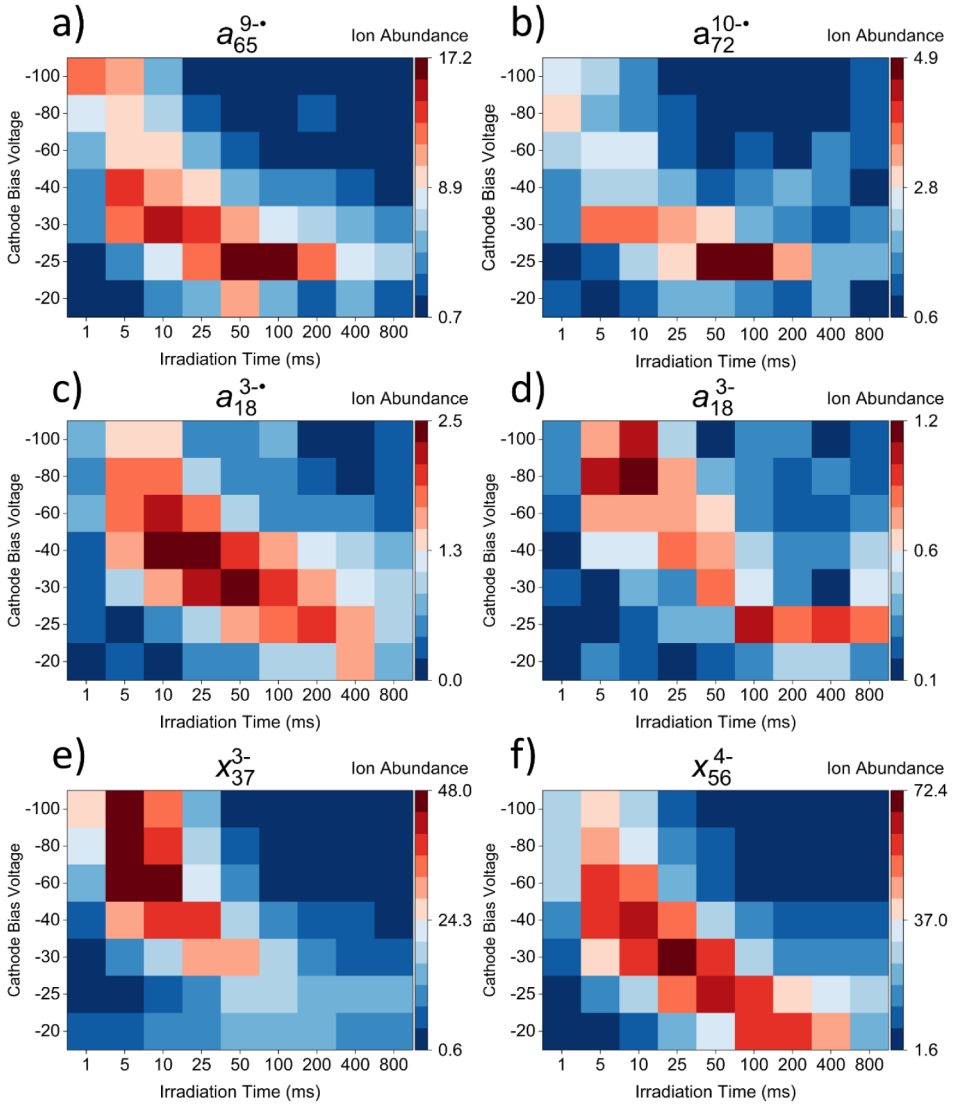


Figure 4. Abundance heatmaps from selected β-casein EDD fragment ions as functions of cathode bias voltage and irradiation time. Experimental conditions: 2.5 μM, 100 scans, +5 V offset on the electron extraction grid relative to the cathode bias voltage. a) $a_{65}^{9-\bullet}$; b) $a_{72}^{10-\bullet}$; c) $a_{18}^{3-\bullet}$; d) a_{18}^{3-}; e) x_{37}^{3-}; f) x_{56}^{4-}.

ICR instrument, resulting in a sequence coverage of ~36% at optimized conditions (−30 cathode bias voltage, 900 ms irradiation; Figure S5). Despite the lower sequence coverage compared with β-casein, seven of the phosphoserine locations could be unambiguously determined across the 9 known sites. The eighth phosphoserine could be narrowed down to two possible residues, only one of which is a known phosphorylation site. The EDD data also revealed that serine 41, the most N-terminal of the known α-casein phosphoserine sites was not modified in the isolated proteoform. In EDD of α-casein, backbone cleavages were not observed within the phosphorylation dense region. However, compared with β-casein, this region is located further from the N-terminus and thus may be more difficult to access. The lower sequence coverage as compared to β-casein, despite fewer residues, may be attributed to the higher number of phosphoserine residues, which may form stabilizing salt bridges within the protein that contribute to a lower degree of fragmentation.

Electron Energy and Irradiation Time Effects in Top-Down EDD

Because the three different casein experiments on the custom instrument showed different optima for the cathode bias voltage and irradiation time, these two parameters were further examined across 63 conditions to generate β-casein fragment ion abundance heatmaps. Example heatmaps for six different fragment ions are shown in Figure 4. As described above, β-casein EDD was dominated by $a/a\bullet$-type fragments, presumably due to the high density of acidic sites in the N-terminal region of the protein. For larger, highly charged $a\bullet$ ions, e.g., $a_{65}^{9-\bullet}$ (Figure 4a) and $a_{72}^{10-\bullet}$ (Figure 4b), abundance is highest below −30 cathode bias voltage, corresponding to an electron energy of ~25 eV (Figure 1) and 50−200 ms irradiation. At higher electron energy, these larger fragments may undergo secondary fragmentation to yield smaller fragments. Consistently, the smaller, lower charge state $a_{18}^{3-\bullet}$ shows the highest abundance at ~−40 cathode bias voltage (~33 eV electrons; Figure 4c). Its even-electron counterpart, a_{18}^{3-}, shows the highest abundance at further

https://doi.org/10.1021/jasms.6c00260
J. Am. Soc. Mass Spectrom. XXXX, XXX, XXX−XXX

Downloaded from pubs.acs.org/jamsef/article-pdf/doi/10.1021/jasms.6c00260/6901816/jasms.6c00260.pdf by FLORIDA STATE UNIV user on 02 November 2026

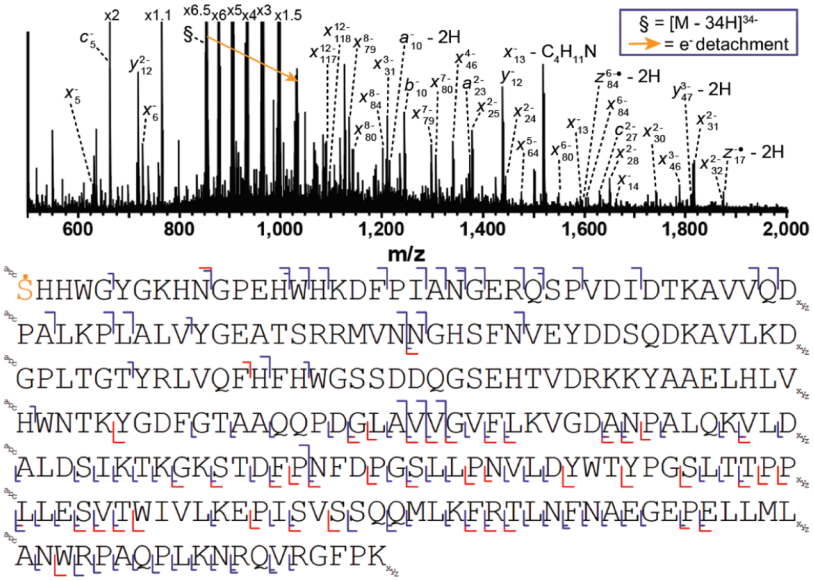


Figure 5. Top) EDD spectrum from the 34− charge state of carbonic anhydrase II with some fragment ion annotations. The "§" denotes the precursor ion. Bottom) Sequence coverage map wherein purple brackets represent cleavage site for expected backbone fragment ions, while red brackets represent (y − 2H) fragment ions or other fragments with ≥2 hydrogen loss. The N-acetyl serine is in orange and marked with a square. 120/258 cleavage sites were observed for ∼47% sequence coverage. Experimental conditions: 5 μM, 200 scans, quadrupole + SWIFT isolation, −80 cathode bias voltage −75 electron extraction grid voltage, 35 ms irradiation.

increased cathode bias voltage (−80 V or ∼72 eV electrons) and short irradiation time (5−10 ms; Figure 4d). A second maximum is observed around −25 cathode bias voltage (∼20 eV electrons) but at much longer irradiation time (100−800 ms), suggesting vibrational activation to eject a hydrogen radical from the $a_{18}^{3-\bullet}$ ion is occurring through an accompanying negative electron induced dissociation (nEInD) mechanism.[59] The higher electron energy needed to maximize abundance of the x_{37}^{3-} fragment (Figure 4e) may have two explanations: either higher energy is needed to achieve electron ejection from the C-terminal portion of β-casein due to the lower density of acidic sites, or this ion is a secondary fragment from larger product ions. By contrast, the x_{56}^{4-} fragment (Figure 4f) appears in an energy regime that most closely matches $a_{65}^{9-\bullet}$ (Figure 4a), demonstrating that not all *x*-type fragments require high electron energy to appear. Notably, x_{56}^{4-} is present even at the −20 cathode bias voltage, which may be due to its high abundance.

The observation that highly charged fragments are more abundant at lower electron energy and longer irradiation times was further examined by generating heatmaps for the x_{133} fragment at different charge states, ranging from 10− to 14− (Figure S6). These heatmaps show a clear trend of diminishing abundance of the x_{133} higher charge states with increasing electron energy in favor of lower charges states. However, for optimum abundance of the lower charge states, irradiation times must be shortened. Based on these findings, titration of irradiation time can be used to generate the most informative EDD spectra in each energy regime. Importantly, at high electron energy, spectra can be generated at a fraction of the time required at low energy. For example, −25 cathode bias voltage, 200 ms irradiation shows 49% sequence coverage vs 41% at −80 cathode bias voltage, 5 ms irradiation for the 24− charge state of β-casein (Figures S7 and S8). Moderately higher energy β-casein EDD was also performed on the commercial Bruker instrument at the highest implemented −30 cathode bias voltage vs the aforementioned −20 V. This higher energy regime showed 50% sequence coverage at a 10-fold lower irradiation time (70 ms; Figure S9).

To further explore differences between high- and low-energy EDD, we subjected the 9− charge state of ubiquitin to both the typical[40] ∼15 eV electron energy and to ∼72 eV electrons. Similar to the β-casein results, ∼350 ms irradiation was optimal for the lower electron energy (Figure S10, Top) but, at higher energy, efficient EDD was observed at 20 ms (Figure S10, Bottom). The ubiquitin sequence coverage was identical (∼81%) at both experimental conditions; however, because each condition generated a few unique backbone bond cleavages, a total sequence coverage of 88% from 66/75 possible cleavage sites was obtained from the combined data. The type of observed fragment ions ($a/c/x/(y-2H)/z/(z-2H)$) did not appear to change with electron energy.

This inverse relationship between cathode bias voltage and irradiation time can be explained by both electron flux and energy: as cathode bias voltage increases, the number of generated electrons also increases and, to compensate for the increased electron flux, irradiation times must be shortened. Too many electrons result in space charge limitations and overfragmentation. However, increased electron flux alone does not appear to fully account for the extent of irradiation time reduction at optimum EDD efficiency. For example, a current of 33 μA was observed at −25 cathode bias voltage, whereas 59 μA was generated at −80 V, an ∼3× increase (Figure S2). By contrast, the optimum irradiation times at these two conditions were 200 vs 5 ms, a 40× decrease. Furthermore, at electron energies >70 eV, an excessive amount of energy is available for electron ejection from multiply charged polyanions, such as proteins or nucleic acids with dozens of negative charges. A single high energy electron may deposit energy into multiple analyte anions, or result in multiple electron ejections from the same analyte. Alternatively, electron ejection may be accompanied by higher order structure unfolding that may lead to release of additional fragment ions such as the x_{37}^{3-} in Figure 4e.

Downloaded from pubs.acs.org/jamsef/article-pdf/doi/10.1021/jasms.6c00260/6901816/jasms.6c00260.pdf by FLORIDA STATE UNIV user on 02 November 2026

https://doi.org/10.1021/jasms.6c00260
J. Am. Soc. Mass Spectrom. XXXX, XXX, XXX−XXX

Following our discovery that EDD yielded analytically useful sequence coverage for ~24 kDa caseins with ~72 eV electrons at irradiation times as short as 5 ms, we subjected the 34− charge state of bovine carbonic anhydrase (CAII, ~29 kDa, estimated pI ~ 6.22[15]) to high energy EDD. At −80 cathode bias voltage (corresponding to ~72 eV electrons; Figure 1) no fragments were observed in single scan spectra with an irradiation time of 5 ms. This lack of fragment ion signal is likely due to the larger protein size compared with β-casein, spreading available ion current over a higher number of fragmentation pathways. Low charge state fragments were observed at an irradiation time of 35 ms. Signal averaging under these conditions resulted in the spectrum shown in Figure 5, Top. This higher energy EDD resulted in 47% sequence coverage (Figure 5, Bottom).

A bottleneck for wider adaptation of EDD in biomolecular analysis has been the relatively long irradiation time, which is suboptimal for coupling with liquid chromatography. Long irradiation times prevent averaging of a high number of scans across an LC elution time and thus preclude optimal S/N ratio based on the square root increase vs number of averaged scans. Kjeldsen and coworkers demonstrated LC-EDD for bottom-up proteomic analysis with 150−170 ms irradiation times but peptide sequence coverage was limited to <30%.[63] Recently, efficient oligonucleotide EDD has been shown with 10 ms irradiation in a plasma configuration with a magneto radiofrequency ion trap, and with 55 ms irradiation in an Omnitrap configuration.[23,36] With the ability to achieve efficient intact protein EDD at 20−35 ms irradiation time with high energy (~72 eV) electrons, we also examined EDD of the 18 nt, unmodified antisense therapeutic, Nusinersen, at this previously unexplored energy range. For this molecule we evaluated EDD efficiency by measuring the abundance of six different fragment ions (d_5^{2-}, w_5^{2-}, d_{12}^{5-}, w_{13}^{2-}, w_{16}^{6-}, and w_{17}^{6-}) from the quadrupole isolated 8− charge state as a function of electron irradiation time (1−800 ms) at four different cathode bias voltages (−20 V, −25 V, −30 V and −100 V), as shown in Figure S11. The trend observed for proteins that increased electron energy allows for shorter irradiation time also holds for this oligonucleotide. While −30 cathode bias voltage provided the highest fragment ion abundance with 100−250 ms irradiation, −100 cathode bias voltage (~92 eV electrons) allowed an irradiation time as low as 3 ms, yielding 30−60% of the fragment ion abundance at 1.2−3% of the time. Full sequence coverage was obtained (100%; Figure 6, Top). The corresponding mass spectrum is shown in Figure 6, Bottom. These EDD conditions resulted in 17/17 interresidue bond cleavages, exclusively from d/w-type fragment ions although several c/y-type ions (which suggest accompanying vibrational activation[22,64]) were also observed at lower abundance. With the exception of neutral nucleobase loss from charge-reduced precursor ions, neutral losses from fragment ions were virtually absent. The irradiation time of 3 ms is the lowest reported for EDD, outperforming other instrument configurations.[23,36]

Top-Down Protein EDD vs UVPD

While annotating protein EDD spectra, we noticed that (y − 2H) fragments were prevalent, but only from backbone bond cleavage N-terminal to, or near proline residues, as summarized in Supporting Table 1. Specifically, as shown in Figure S12, (y − 2H) fragments appear at 20/35, 9/19, and 3/3 proline residues for β-casein, CAII, and ubiquitin, respectively. This

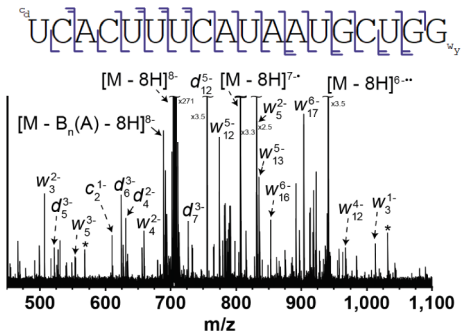


Figure 6. EDD of the 8− charge state of unmodified Nusinersen RNA. Sequence coverage with assigned fragment ions is denoted above the spectrum. Experimental conditions: 16 μM, −100 cathode bias voltage, −95 grid voltage, 3 ms irradiation, 100 scans. * = Electronic noise.

fragment ion type is also sparsely generated at nonproline cleavage sites. Specifically, three, one, and three annotated (y − 2H) ions originated near residues other than proline for β-casein, CAII, and ubiquitin, respectively. Figure 7 shows two zoomed-in regions from the β-casein EDD spectrum in Figure 2, illustrating the assignment of $(y_{36} - 2H)^{3-}$ (Left) and $(y_{52} - 2H)^{4-}$ (Right). y-type fragments are typically of low abundance in top-down EDD, and hydrogen-deficient (y − 2H) fragments have not previously been reported for intact protein EDD. By contrast, this fragment ion type has been observed in EDD and nEInD of peptides,[61,65] but its formation mechanism has not been addressed. Generation of typical and singly hydrogen deficient, radical y-type fragments from backbone cleavage N-terminal to proline in peptide EDD, has been attributed to charge directed dissociation from vibrational activation associated with nEInD,[59] which also occurs under EDD conditions.[66] By contrast, (y − nH) fragment ions, where $n \geq 2$, are common in UVPD. These fragment ion types have been proposed to originate from electronic excitation of precursor ions.[67,68] Similarly, the numerous (y − 2H) fragments observed here from top-down EDD may originate from electronically excited states, populated upon energy transfer from the relatively high energy electrons. While the proposed UVPD mechanism of fragmentation from higher electronic states also involves formation of possible b-, (b + 2H)-, and (a + 2H)-type ions,[67] empirically, EDD does not appear to produce such fragments.

To explore the optimum conditions for the production of (y − 2H)-type fragments, a heatmap was generated for the $(y_{36} - 2H)^{3-}$ fragment. This heatmap (Figure S13) shows a bimodal distribution, with highest abundance at −60 cathode bias voltage (~52 eV electrons) and 5−10 ms irradiation as well as −25 cathode bias voltage (~20 eV electrons) and 50−100 ms irradiation. Overall, the highest abundance of this (y − 2H) fragment appears to occur in a similar parameter space as the $a_{18}^{3-\bullet}$ ion in Figure 4c, an interesting finding considering the established assumption that radical a-type ions originate from radical-driven fragmentation (such as EDD) but not necessarily electronic excitation. On the other hand, again, nEInD and EDD are known to occur simultaneously.[66]

Based on our finding that (y − 2H) fragments are prevalent in EDD spectra, similar to established top-down UVPD,[68] we acquired EDD on the custom instrument for additional proteins with published UVPD spectra: apocalmodulin (~16.7 kDa, including N-terminal acetylation and one lysine

Downloaded from pubs.acs.org/jamsef/article-pdf/doi/10.1021/jasms.6c00260/6901816/jasms.6c00260.pdf by FLORIDA STATE UNIV user on 02 November 2026

https://doi.org/10.1021/jasms.6c00260
J. Am. Soc. Mass Spectrom. XXXX, XXX, XXX−XXX

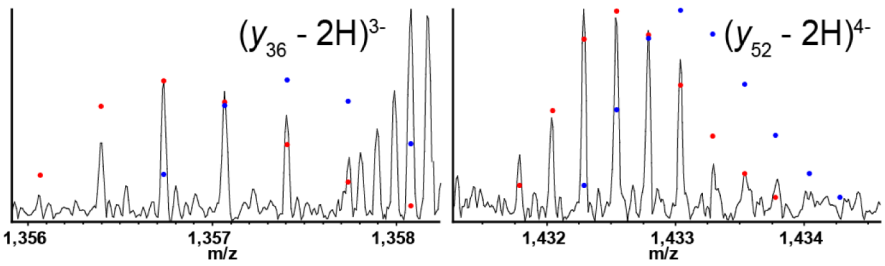


Figure 7. Zoomed-in regions of the β-casein EDD spectrum in Figure 2. (y − 2H) fragments were commonly observed from backbone cleavage at the N-terminal side of proline. Such fragments have been proposed to originate from electronic excitation in UVPD. Assignments of $(y_{36} - 2H)^{3-}$ and $(y_{52} - 2H)^{4-}$ fragments based on their theoretical isotopic distributions (red dots) are shown. Calculated isotopic distributions for the corresponding y-type ions are also included (blue dots).

trimethylation)[69] and enolase (~46 kDa).[26] For apocalmodulin, the 17− charge state was fragmented, resulting in 57% sequence coverage (Figure S14). Interestingly, EDD of apocalmodulin nearly exclusively generated complementary series of *a*/*x* fragment ions, making spectral interpretation straightforward. In comparison, 193 nm UVPD of 7+ unmodified apocalmodulin[69] resulted in slightly lower sequence coverage (55%). Also, diverse fragment ion types, including *a*/*b*/*c*/*x*/*y*/*z*-type fragments, were generated, potentially complicating data analysis. Recent negative ion mode 193 nm UVPD of ubiquitin demonstrated ~95% sequence coverage,[26] whereas combining fragments from both −20 and −80 cathode bias voltage EDD experiments (Figure S10) results in 88%. For carbonic anhydrase II, previous 193 nm UVPD generated ~40% sequence coverage,[26] while our high energy EDD generated 49% (Figure 5). We also performed EDD of the larger, ~46 kDa protein enolase at both high and low energy (Figure S15). The high energy method generated an extensive series of 1 *m*/*z* spaced,[70] so-called "picket fence" peaks[71] with minimal observation of annotatable fragment ions, while the low energy method showed less prominent picket fence peaks along with 16/435 annotatable fragments, or ~4% sequence coverage. By comparison, 193 nm UVPD of enolase anions generated notably higher, ~40%, sequence coverage.[26] Interestingly, the primarily *a*-type fragments observed in EDD of enolase (Figure S15) are as large as 111 residues, indicating electron access to the protein interior, despite the dearth of assignable terminal fragments.

For a highly charged protein such as enolase 55−, multiple electron ejection is energetically favorable with 6 electron detachment events observed at −25 cathode bias voltage (Figure S15). Such multiple electron detachment events from a single protein anion may generate more than one radical site, which may cause internal fragment formation. At high electron energy, secondary fragmentation of larger fragment ions likely generates additional internal fragments and, thus, would explain the more prominent "picket fence" peaks at high vs low energy EDD. As described in an accompanying paper in this issue,[71] such picket fence peaks originate from constructive interference of a high number of diverse terminal and internal fragments with overlapping *m*/*z* ratios. Increased secondary fragmentation at higher electron energy is also evident from the ubiquitin EDD in Figure S10. Here, the main difference between the spectra acquired at higher and lower electron energy is the average fragment ion charge state: −4.6 at −20 cathode bias voltage and −3.8 at −80 cathode bias voltage, a difference of ~20%. A decrease in overall fragment ion charge, presumably from higher order fragmentation of larger, highly charged fragments decreases access to the protein interior but may improve sequence coverage near the protein termini.

Another similarity between the top-down EDD spectra presented here and published UVPD data is that backbone cleavage sites are not clustered around basic residues, contrary to previously reported protein EDD.[28] On the other hand, previous work also showed a trend of increasing sequence coverage with decreasing protein size with the highest sequence coverage at 2.8 kDa, i.e., the higher sequence coverage could also be due to the much smaller number of possible interresidue bond cleavage sites. For apocalmodulin, nearly all fragments are observed ~70 residues from the N-terminus and 37 residues from the C-terminus, i.e., sequence coverage appears limited by the lack of large fragment ions from the protein interior, presumably due to overfragmentation. It has been proposed that electron ejection in EDD occurs from acidic sites,[72] i.e., in a linear biopolymer fragmentation should be favored at such sites. However, because proteins are charge-solvated in the gas phase, there will be other amino acids nearby for radical migration.

CONCLUSION

EDD is shown to provide vastly improved sequence coverage for intact proteins as compared to previous literature data due to several factors. First, the ICR cells used in this work; an electrically compensated open cell and a commercially available dynamically harmonized cell, have higher volume and thus offer superior space charge capacity than previous Infinity cells used for EDD in FT-ICR instrumentation. Second, further space charge capacity improvement was gained with higher magnet field; 9.4 T versus earlier experiments at 7 T. Third, the on-axis 1.016 cm diameter solid cathode provided increased ion-electron overlap, as compared to the hollow cathodes used previously. EDD resulted in backbone bond cleavage between sequential β-casein phosphoserine residues without neutral phosphoric acid loss. The sequence coverage for β-casein was improved by an order of magnitude or more compared with previous reports. Up to 29 kDa proteins demonstrated analytically useful sequence coverage by EDD. Top-down EDD revealed prevalent (*y* − 2H) fragments, which constitute evidence of precursor ion electronic excitation in EDD. Heatmaps were generated to demonstrate the inverse relationship between electron energy and irradiation time. An 18-mer RNA was demonstrated to show full sequence coverage (17/17 backbone cleavage sites) with a 3 ms irradiation time employing high (~92 eV) energy electrons. Future work will focus on EDD of larger oligonucleotides in an LC-EDD workflow.

https://doi.org/10.1021/jasms.6c00260
J. Am. Soc. Mass Spectrom. XXXX, XXX, XXX−XXX

Downloaded from pubs.acs.org/jamsef/article-pdf/doi/10.1021/jasms.6c00260/6901816/jasms.6c00260.pdf by FLORIDA STATE UNIV user on 02 November 2026

■ ASSOCIATED CONTENT

Data Availability Statement

Raw data files are available for download from the Open Science Framework (OSF): https://doi.org/10.17605/OSF.IO/8F659.

Supporting Information

The Supporting Information is available free of charge at https://pubs.acs.org/doi/10.1021/jasms.6c00260.

Figure S1: ICR cells and cathodes used for EDD; Figure S2: measured current on the transfer quadrupole; Figure S3: broadband β-casein EDD sequence coverage; Figure S4: β-casein MS^1 and major proteoforms; Figure S5: EDD of octuply phosphorylated α-casein 23−; Figure S6: charge state heatmaps for the β-casein x_{133} fragment ion; Figure S7: β-casein 24−, −25 cathode bias voltage EDD sequence coverage; Figure S8: β-casein 24−, −80 cathode bias voltage EDD sequence coverage; Figure S9: β-casein 24−, −30 cathode bias voltage Bruker EDD sequence coverage; Figure S10: EDD of ubiquitin 9− at −20 and −80 cathode bias voltages; Figure S11: energy and irradiation time dependence for the Nusinersen RNA; Figure S12: sequence maps highlighting proline and $(y - 2H)$ fragments; Figure S13: heatmap for the β-casein $(y_{36}^{3-} - 2H)$ fragment ion; Figure S14: EDD of calmodulin 17−; Figure S15: EDD of enolase 55− at −20 and −80 cathode bias voltages; Table S1: Table of $(y - 2H)$ fragments from EDD (PDF)

■ AUTHOR INFORMATION

Corresponding Author

Kristina Håkansson − *Ion Cyclotron Resonance Program, National High Magnetic Field Laboratory, Tallahassee, Florida 32310-4005, United States; Department of Chemistry & Biochemistry, Florida State University, Tallahassee, Florida 32306-4390, United States;* orcid.org/0000-0003-1926-0542; Email: khakansson@magnet.fsu.edu

Authors

Steven A. DeFiglia − *Ion Cyclotron Resonance Program, National High Magnetic Field Laboratory, Tallahassee, Florida 32310-4005, United States; Department of Chemistry & Biochemistry, Florida State University, Tallahassee, Florida 32306-4390, United States*

Nathan K. Kaiser − *Ion Cyclotron Resonance Program, National High Magnetic Field Laboratory, Tallahassee, Florida 32310-4005, United States*

Greg T. Blakney − *Ion Cyclotron Resonance Program, National High Magnetic Field Laboratory, Tallahassee, Florida 32310-4005, United States;* orcid.org/0000-0002-4205-9866

Marek Polák − *Ion Cyclotron Resonance Program, National High Magnetic Field Laboratory, Tallahassee, Florida 32310-4005, United States;* orcid.org/0000-0002-8929-5479

Complete contact information is available at: https://pubs.acs.org/10.1021/jasms.6c00260

Notes

The authors declare no competing financial interest.

■ ACKNOWLEDGMENTS

This work was supported by NSF Grant CHE2528759 to K.H. A portion of the work was performed at the Ion Cyclotron Resonance User Facility at the National High Magnetic Field Laboratory at Florida State University, supported by the National Science Foundation Divisions of Materials Research and Chemistry (DMR-2128556) and by the State of Florida. Chad R. Weisbrod, Lissa C. Anderson, and Sean D. Dunham are thanked for helpful discussions. John P. Quinn, Christopher Wootton, and Alina Theisen are thanked for assistance with the FT-ICR instruments. This article was written in honor of Alan G. Marshall, with the majority of data acquired on the original (upgraded) flagship instrument of his FT-ICR program at the National High Magnetic Field Laboratory. N. K. K., G. T. B., and K. H. are indebted to Dr. Marshall for his mentorship and support spanning 25 years.

■ REFERENCES

(1) Miller, R. M.; Smith, L. M. Overview and Considerations in Bottom-up Proteomics. *Analyst* **2023**, *148* (3), 475−486.

(2) Wolters, D. A.; Washburn, M. P.; Yates, J. R. An Automated Multidimensional Protein Identification Technology for Shotgun Proteomics. *Anal. Chem.* **2001**, *73* (23), 5683−5690.

(3) Link, A. J.; Eng, J.; Schieltz, D. M.; Carmack, E.; Mize, G. J.; Morris, D. R.; Garvik, B. M.; Yates, J. R. Direct Analysis of Protein Complexes Using Mass Spectrometry. *Nat. Biotechnol.* **1999**, *17* (7), 676−682.

(4) Fitzgerald, N. J.; Huang, W.; Clark, K. D. RNA Sample Preparation Strategies for Mass Spectrometry Sequencing of the Epitranscriptome and Therapeutic RNAs: A Review. *Anal. Chim. Acta.* **2026**, *1393*, 345154.

(5) Arnesen, T. Towards a Functional Understanding of Protein N-Terminal Acetylation. *PLoS Biol.* **2011**, *9* (5), No. e1001074.

(6) Aebersold, R.; Agar, J. N.; Amster, I. J.; Baker, M. S.; Bertozzi, C. R.; Boja, E. S.; Costello, C. E.; Cravatt, B. F.; Fenselau, C.; Garcia, B. A.; Ge, Y.; Gunawardena, J.; Hendrickson, R. C.; Hergenrother, P. J.; Huber, C. G.; Ivanov, A. R.; Jensen, O. N.; Jewett, M. C.; Kelleher, N. L.; Kiessling, L. L.; Krogan, N. J.; Larsen, M. R.; Loo, J. A.; Ogorzalek Loo, R. R.; Lundberg, E.; MacCoss, M. J.; Mallick, P.; Mootha, V. K.; Mrksich, M.; Muir, T. W.; Patrie, S. M.; Pesavento, J. J.; Pitteri, S. J.; Rodriguez, H.; Saghatelian, A.; Sandoval, W.; Schlüter, H.; Sechi, S.; Slavoff, S. A.; Smith, L. M.; Snyder, M. P.; Thomas, P. M.; Uhlén, M.; Van Eyk, J. E.; Vidal, M.; Walt, D. R.; White, F. M.; Williams, E. R.; Wohlschlager, T.; Wysocki, V. H.; Yates, N. A.; Young, N. L.; Zhang, B. How Many Human Proteoforms Are There? *Nat. Chem. Biol.* **2018**, *14* (3), 206−214.

(7) Roberts, D. S.; Loo, J. A.; Tsybin, Y. O.; Liu, X.; Wu, S.; Chamot-Rooke, J.; Agar, J. N.; Paša-Tolić, L.; Smith, L. M.; Ge, Y. Top-down Proteomics. *Nat. Rev. Methods Primers* **2024**, *4* (1), 38.

(8) Srzentić, K.; Fornelli, L.; Tsybin, Y. O.; Loo, J. A.; Seckler, H.; Agar, J. N.; Anderson, L. C.; Bai, D. L.; Beck, A.; Brodbelt, J. S.; Van Der Burgt, Y. E. M.; Chamot-Rooke, J.; Chatterjee, S.; Chen, Y.; Clarke, D. J.; Danis, P. O.; Diedrich, J. K.; D'ippolito, R. A.; Dupré, M.; Gasilova, N.; Ge, Y.; Goo, Y. A.; Goodlett, D. R.; Greer, S.; Haselmann, K. F.; He, L.; Hendrickson, C. L.; Hinkle, J. D.; Holt, M. V.; Hughes, S.; Hunt, D. F.; Kelleher, N. L.; Kozhinov, A. N.; Lin, Z.; Malosse, C.; Marshall, A. G.; Menin, L.; Millikin, R. J.; Nagornov, K. O.; Nicolardi, S.; Paša-Tolić, L.; Pengelley, S.; Quebbemann, N. R.; Resemann, A.; Sandoval, W.; Sarin, R.; Schmitt, N. D.; Shabanowitz, J.; Shaw, J. B.; Shortreed, M. R.; Smith, L. M.; Sobott, F.; Suckau, D.; Toby, T.; Weisbrod, C. R.; Wildburger, N. C.; Yates, J. R.; Yoon, S. H.; Young, N. L.; Zhou, M. Interlaboratory Study for Characterizing Monoclonal Antibodies by Top-Down and Middle-Down Mass Spectrometry. *J. Am. Soc. Mass Spectrom.* **2020**, *31* (9), 1783−1802.

(9) Taucher, M.; Breuker, K. Characterization of Modified RNA by Top-Down Mass Spectrometry. *Angew. Chem., Int. Ed.* **2012**, *51* (45), 11289−11292.

Downloaded from pubs.acs.org/jamsse/article-pdf/doi/10.1021/jasms.6c00260/6901816/jasms.6c00260.pdf by FLORIDA STATE UNIV user on 02 November 2026

(10) Ntai, I.; Fornelli, L.; De Hart, C. J.; Hutton, J. E.; Doubleday, P. F.; Le Duc, R. D.; Van Nispen, A. J.; Fellers, R. T.; Whiteley, G.; Boja, E. S.; Rodriguez, H.; Kelleher, N. L. Precise Characterization of KRAS4b Proteoforms in Human Colorectal Cells and Tumors Reveals Mutation/Modification Cross-Talk. *Proc. Natl. Acad. Sci. U. S. A.* **2018**, *115* (16), 4140−4145.
(11) Schaffer, L. V.; Anderson, L. C.; Butcher, D. S.; Shortreed, M. R.; Miller, R. M.; Pavelec, C.; Smith, L. M. Construction of Human Proteoform Families from 21 T Fourier Transform Ion Cyclotron Resonance Mass Spectrometry Top-Down Proteomic Data. *J. Proteome Res.* **2021**, *20* (1), 317−325.
(12) Ge, Y.; Lawhorn, B. G.; ElNaggar, M.; Strauss, E.; Park, J.-H.; Begley, T. P.; McLafferty, F. W. Top Down Characterization of Larger Proteins (45 kDa) by Electron Capture Dissociation Mass Spectrometry. *J. Am. Chem. Soc.* **2002**, *124* (4), 672−678.
(13) Polák, M.; Yassaghi, G.; Kavan, D.; Filandr, F.; Fiala, J.; Kukačka, Z.; Halada, P.; Loginov, D. S.; Novák, P. Utilization of Fast Photochemical Oxidation of Proteins and Both Bottom-up and Top-down Mass Spectrometry for Structural Characterization of a Transcription Factor−dsDNA Complex. *Anal. Chem.* **2022**, *94* (7), 3203−3210.
(14) Dunham, S. D.; Brodbelt, J. S. Enhancing Top-Down Analysis of Proteins by Combining Ultraviolet Photodissociation (UVPD), Proton-Transfer Charge Reduction (PTCR), and Gas-Phase Fractionation to Alleviate the Impact of Nondissociated Precursor Ions. *J. Am. Soc. Mass Spectrom.* **2024**, *35* (2), 255−265.
(15) Kozlowski, L.-P.-P. pI 2.0: Proteome Isoelectric Point Database Update. *Nucleic Acids Res.* **2022**, *50* (D1), D1535−D1540.
(16) Bhide, G. P.; Colley, K. J. Sialylation of N-Glycans: Mechanism, Cellular Compartmentalization and Function. *Histochem. Cell Biol.* **2017**, *147* (2), 149−174.
(17) Zhu, W.; Zhou, Y.; Guo, L.; Feng, S. Biological Function of Sialic Acid and Sialylation in Human Health and Disease. *Cell Death Discovery* **2024**, *10* (1), 415.
(18) Yang, Y.-S.; Wang, C.-C.; Chen, B.-H.; Hou, Y.-H.; Hung, K.-S.; Mao, Y.-C. Tyrosine Sulfation as a Protein Post-Translational Modification. *Molecules* **2015**, *20* (2), 2138−2164.
(19) Peterson, R. T.; Schreiber, S. L. Kinase Phosphorylation: Keeping It All in the Family. *Curr. Biol.* **1999**, *9* (14), R521−R524.
(20) Ardito, F.; Giuliani, M.; Perrone, D.; Troiano, G.; Muzio, L. L. The Crucial Role of Protein Phosphorylation in Cell Signaling and Its Use as Targeted Therapy (Review). *Int. J. Mol. Med.* **2017**, *40* (2), 271−280.
(21) Macias, L. A.; Garcia, S. P.; Back, K. M.; Wu, Y.; Johnson, G. H.; Kathiresan, S.; Bellinger, A. M.; Rohde, E.; Freitas, M. A.; Madsen, J. A. Spacer Fidelity Assessments of Guide RNA by Top-Down Mass Spectrometry. *ACS Cent. Sci.* **2023**, *9* (7), 1437−1452.
(22) Taucher, M.; Breuker, K. Top-down Mass Spectrometry for Sequencing of Larger (up to 61 Nt) RNA by CAD and EDD. *J. Am. Soc. Mass Spectrom.* **2010**, *21* (6), 918−929.
(23) Rosu, F.; Chiba, R.; Mallika, A. M.; Smyrnakis, A.; Greisch, J.-F.; Papanastasiou, D.; Gabelica, V. Activation of Oligonucleotide Polyanions Using Collisions, Electrons and Photons in a timsOmni Platform. *J. Am. Soc. Mass Spectrom.* **2026**, *37* (6), 1342−1352.
(24) Kellersberger, K. A.; Yu, E.; Kruppa, G. H.; Young, M. M.; Fabris, D. Top-Down Characterization of Nucleic Acids Modified by Structural Probes Using High-Resolution Tandem Mass Spectrometry and Automated Data Interpretation. *Anal. Chem.* **2004**, *76* (9), 2438−2445.
(25) Baba, T.; Karasawa, K. Sequencing of DNA Mixtures Using Liquid Chromatography—Postactivated Plasma Electron Detachment Dissociation Mass Spectrometry. *Anal. Chem.* **2025**, *97* (33), 18235−18242.
(26) Ren, H.; Brodbelt, J. S. Top-Down Characterization of Protein Anions Using Ultraviolet Photodissociation Mass Spectrometry. *J. Am. Soc. Mass Spectrom.* **2026**, *37* (4), 884−893.
(27) Song, H.; Håkansson, K. Electron Detachment Dissociation and Negative Ion Infrared Multiphoton Dissociation of Electrosprayed Intact Proteins. *Anal. Chem.* **2012**, *84* (2), 871−876.
(28) Ganisl, B.; Valovka, T.; Hartl, M.; Taucher, M.; Bister, K.; Breuker, K. Electron Detachment Dissociation for Top-Down Mass Spectrometry of Acidic Proteins. *Chem.Eur. J.* **2011**, *17* (16), 4460−4469.
(29) Dunham, S. D.; Wei, B.; Lantz, C.; Loo, J. A.; Brodbelt, J. S. Impact of Internal Fragments on Top-Down Analysis of Intact Proteins by 193 Nm UVPD. *J. Proteome Res.* **2023**, *22* (1), 170−181.
(30) Fornelli, L.; Srzentić, K.; Toby, T. K.; Doubleday, P. F.; Huguet, R.; Mullen, C.; Melani, R. D.; dos Santos Seckler, H.; De Hart, C. J.; Weisbrod, C. R.; et al. Thorough Performance Evaluation of 213 nm Ultraviolet Photodissociation for Top-down Proteomics. *Mol. Cell. Proteomics* **2020**, *19* (2), 405−420.
(31) Zubarev, R. A.; Kelleher, N. L.; McLafferty, F. W. Electron Capture Dissociation of Multiply Charged Protein Cations. A Nonergodic Process. *J. Am. Chem. Soc.* **1998**, *120* (13), 3265−3266.
(32) DeFiglia, S. A.; Szot, C. W.; Håkansson, K. Negative-Ion Electron Capture Dissociation of MALDI-Generated Peptide Anions. *Anal. Chem.* **2024**, *96* (21), 8800−8806.
(33) Nesbitt, D. J.; Mertz, K. L.; Probasco, M. D.; Peters-Clarke, T. M.; Oman, T. J.; Syka, J. E. P.; Quarmby, S. T.; Coon, J. J. Implementation of Infrared-Activated Negative Electron Transfer Dissociation (IR-NETD) Using Xenon on a Quadrupole-Orbitrap-Quadrupole Linear Ion Trap Mass Spectrometer. *J. Am. Soc. Mass Spectrom.* **2026**, *37* (1), 301−309.
(34) Peters-Clarke, T. M.; Quan, Q.; Brademan, D. R.; Hebert, A. S.; Westphall, M. S.; Coon, J. J. Ribonucleic Acid Sequence Characterization by Negative Electron Transfer Dissociation Mass Spectrometry. *Anal. Chem.* **2020**, *92* (6), 4436−4444.
(35) Budnik, B. A.; Haselmann, K. F.; Zubarev, R. A. Electron Detachment Dissociation of Peptide Di-Anions: An Electron−Hole Recombination Phenomenon. *Chem. Phys. Lett.* **2001**, *342* (3), 299−302.
(36) Karasawa, K.; Duchoslav, E.; Baba, T. Fast Electron Detachment Dissociation of Oligonucleotides in Electron-Nitrogen Plasma Stored in Magneto Radio-Frequency Ion Traps. *Anal. Chem.* **2022**, *94* (44), 15510−15517.
(37) Caravatti, P.; Allemann, M. The 'Infinity Cell': A New Trapped-ion Cell with Radiofrequency Covered Trapping Electrodes for Fourier Transform Ion Cyclotron Resonance Mass Spectrometry. *Org. Mass Spectrom.* **1991**, *26* (5), 514−518.
(38) Tsybin, Y. O.; Witt, M.; Baykut, G.; Kjeldsen, F.; Håkansson, P. Combined Infrared Multiphoton Dissociation and Electron Capture Dissociation with a Hollow Electron Beam in Fourier Transform Ion Cyclotron Resonance Mass Spectrometry. *Rapid Commun. Mass Spectrom.* **2003**, *17* (15), 1759−1768.
(39) Leach, F. E.; Wolff, J. J.; Laremore, T. N.; Linhardt, R. J.; Amster, I. J. Evaluation of the Experimental Parameters Which Control Electron Detachment Dissociation, and Their Effect on the Fragmentation Efficiency of Glycosaminoglycan Carbohydrates. *Int. J. Mass Spectrom.* **2008**, *276* (2), 110−115.
(40) Yang, J.; Håkansson, K. Characterization and Optimization of Electron Detachment Dissociation Fourier Transform Ion Cyclotron Resonance Mass Spectrometry. *Int. J. Mass Spectrom.* **2008**, *276* (2−3), 144−148.
(41) Gorshkov, M. V.; Masselon, C. D.; Nikolaev, E. N.; Udseth, H. R.; Paša-Tolić, L.; Smith, R. D. Considerations for Electron Capture Dissociation Efficiency in FTICR Mass Spectrometry. *Int. J. Mass Spectrom.* **2004**, *234* (1−3), 131−136.
(42) Senko, M. W.; Hendrickson, C. L.; Paša-Tolić, L.; Marto, J. A.; White, F. M.; Guan, S.; Marshall, A. G. Electrospray Ionization Fourier Transform Ion Cyclotron Resonance at 9.4 T. *Rapid Commun. Mass Spectrom.* **1996**, *10* (14), 1824−1828.
(43) Kaiser, N. K.; Quinn, J. P.; Blakney, G. T.; Hendrickson, C. L.; Marshall, A. G. A Novel 9.4 T FTICR Mass Spectrometer with Improved Sensitivity, Mass Resolution, and Mass Range. *J. Am. Soc. Mass Spectrom.* **2011**, *22* (8), 1343−1351.
(44) Wootton, C. A.; Maillard, J.; Theisen, A.; Brabeck, G. F.; Schat, C. L.; Rüger, C. P.; Afonso, C.; Giusti, P. A Gated TIMS FTICR MS

Downloaded from pubs.acs.org/jamsef/article-pdf/doi/10.1021/jasms.6c00260/6901816/jasms.6c00260.pdf by FLORIDA STATE UNIV user on 02 November 2026

Instrument to Decipher Isomeric Content of Complex Organic Mixtures. *Anal. Chem.* **2024**, *96* (28), 11343−11352.
(45) Nikolaev, E. N.; Boldin, I. A.; Jertz, R.; Baykut, G. Initial Experimental Characterization of a New Ultra-High Resolution FTICR Cell with Dynamic Harmonization. *J. Am. Soc. Mass Spectrom.* **2011**, *22* (7), 1125−1133.
(46) Boldin, I. A.; Nikolaev, E. N. Fourier Transform Ion Cyclotron Resonance Cell with Dynamic Harmonization of the Electric Field in the Whole Volume by Shaping of the Excitation and Detection Electrode Assembly. *Rapid Commun. Mass Spectrom.* **2011**, *25* (1), 122−126.
(47) Kaiser, N. K.; Savory, J. J.; McKenna, A. M.; Quinn, J. P.; Hendrickson, C. L.; Marshall, A. G. Electrically Compensated Fourier Transform Ion Cyclotron Resonance Cell for Complex Mixture Mass Analysis. *Anal. Chem.* **2011**, *83* (17), 6907−6910.
(48) Tolmachev, A. V.; Robinson, E. W.; Smith, R. D.; Leach, F. E.; Futrell, J. H.; Paša-Tolić, L. A Conceptual Approach for FT-ICR Cell Harmonization Utilizing External Shim Electrodes. *Int. J. Mass Spectrom.* **2012**, *325*−*327*, 45−50.
(49) Marshall, A. G.; Guan, S. Advantages of High Magnetic Field for Fourier Transform Ion Cyclotron Resonance Mass Spectrometry. *Rapid Commun. Mass Spectrom.* **1996**, *10* (14), 1819−1823.
(50) McFarland, M. A.; Marshall, A. G.; Hendrickson, C. L.; Nilsson, C. L.; Fredman, P.; Månsson, J.-E. Structural Characterization of the GM1 Ganglioside by Infrared Multiphoton Dissociation, Electron Capture Dissociation, and Electron Detachment Dissociation Electrospray Ionization FT-ICR MS/MS. *J. Am. Soc. Mass Spectrom.* **2005**, *16* (5), 752−762.
(51) Tsybin, Y. O.; Quinn, J. P.; Tsybin, O. Y.; Hendrickson, C. L.; Marshall, A. G. Electron Capture Dissociation Implementation Progress in Fourier Transform Ion Cyclotron Resonance Mass Spectrometry. *J. Am. Soc. Mass Spectrom.* **2008**, *19* (6), 762−771.
(52) Håkansson, K.; Chalmers, M. J.; Quinn, J. P.; McFarland, M. A.; Hendrickson, C. L.; Marshall, A. G. Combined Electron Capture and Infrared Multiphoton Dissociation for Multistage MS/MS in a Fourier Transform Ion Cyclotron Resonance Mass Spectrometer. *Anal. Chem.* **2003**, *75* (13), 3256−3262.
(53) Baba, T.; Ryumin, P.; Duchoslav, E.; Chen, K.; Chelur, A.; Loyd, B.; Chernushevich, I. Dissociation of Biomolecules by an Intense Low-Energy Electron Beam in a High Sensitivity Time-of-Flight Mass Spectrometer. *J. Am. Soc. Mass Spectrom.* **2021**, *32* (8), 1964−1975.
(54) Kostyukevich, Y. I.; Vladimirov, G. N.; Nikolaev, E. N. Dynamically Harmonized FT-ICR Cell with Specially Shaped Electrodes for Compensation of Inhomogeneity of the Magnetic Field. Computer Simulations of the Electric Field and Ion Motion Dynamics. *J. Am. Soc. Mass Spectrom.* **2012**, *23* (12), 2198−2207.
(55) Senko, M. W.; Hendrickson, C. L.; Emmett, M. R.; Shi, S. D. H.; Marshall, A. G. External Accumulation of Ions for Enhanced Electrospray Ionization Fourier Transform Ion Cyclotron Resonance Mass Spectrometry. *J. Am. Soc. Mass Spectrom.* **1997**, *8* (9), 970−976.
(56) Wang, T. C. L.; Ricca, T. L.; Marshall, A. G. Extension of Dynamic Range in Fourier Transform Ion Cyclotron Resonance Mass Spectrometry via Stored Waveform Inverse Fourier Transform Excitation. *Anal. Chem.* **1986**, *58* (14), 2935−2938.
(57) Guan, S.; Marshall, A. G. Stored Waveform Inverse Fourier Transform (SWIFT) Ion Excitation in Trapped-Ion Mass Spectrometry: Theory and Applications. *Int. J. Mass Spectrom. Ion Processes* **1996**, *157*−*158*, 5−37.
(58) Chen, B.; Guo, X.; Tucholski, T.; Lin, Z.; McIlwain, S.; Ge, Y. The Impact of Phosphorylation on Electron Capture Dissociation of Proteins: A Top-down Perspective. *J. Am. Soc. Mass Spectrom.* **2017**, *28* (9), 1805−1814.
(59) Pérot-Taillandier, M.; Zirah, S.; Enjalbert, Q.; Antoine, R.; Lemoine, J.; Dugourd, P.; Rebuffat, S.; Tabet, J.; Afonso, C. Prompt and Slow Electron-Detachment-Dissociation/Electron-Photodetachment-Dissociation of a 21-Mer Peptide. *Chem.Eur. J.* **2013**, *19* (1), 350−357.
(60) Haselmann, K. F.; Budnik, B. A.; Kjeldsen, F.; Nielsen, M. L.; Olsen, J. V.; Zubarev, R. A. Electronic Excitation Gives Informative Fragmentation of Polypeptide Cations and Anions. *Eur. J. Mass Spectrom.* **2002**, *8* (2), 117−121.
(61) Hersberger, K. E.; Håkansson, K. Characterization of O -Sulfopeptides by Negative Ion Mode Tandem Mass Spectrometry: Superior Performance of Negative Ion Electron Capture Dissociation. *Anal. Chem.* **2012**, *84* (15), 6370−6377.
(62) Pérot-Taillandier, M.; Afonso, C.; Enjalbert, Q.; Antoine, R.; Dugourd, P.; Cole, R. B.; Tabet, J.-C.; Rebuffat, S.; Zirah, S. Electron Detachment/Photodetachment Dissociation of Lasso Peptides. *Int. J. Mass Spectrom.* **2015**, *390*, 91−100.
(63) Kjeldsen, F.; Hørning, O. B.; Jensen, S. S.; Giessing, A. M. B.; Jensen, O. N. Towards Liquid Chromatography Time-Scale Peptide Sequencing and Characterization of Post-Translational Modifications in the Negative-Ion Mode Using Electron Detachment Dissociation Tandem Mass Spectrometry. *J. Am. Soc. Mass Spectrom.* **2008**, *19* (8), 1156−1162.
(64) McLuckey, S. A.; Van Berker, G. J.; Glish, G. L. Tandem Mass Spectrometry of Small, Multiply Charged Oligonucleotides. *J. Am. Soc. Mass Spectrom.* **1992**, *3* (1), 60−70.
(65) Kalli, A.; Grigorean, G.; Håkansson, K. Electron Induced Dissociation of Singly Deprotonated Peptides. *J. Am. Soc. Mass Spectrom.* **2011**, *22* (12), 2209−2221.
(66) Wolff, J. J.; Laremore, T. N.; Aslam, H.; Linhardt, R. J.; Amster, I. J. Electron Induced Dissociation of Glycosaminoglycan Tetrasaccharides. *J. Am. Soc. Mass Spectrom.* **2008**, *19* (10), 1449−1458.
(67) Girod, M.; Sanader, Z.; Vojkovic, M.; Antoine, R.; MacAleese, L.; Lemoine, J.; Bonacic-Koutecky, V.; Dugourd, P. UV Photodissociation of Proline-Containing Peptide Ions: Insights from Molecular Dynamics. *J. Am. Soc. Mass Spectrom.* **2015**, *26* (3), 432−443.
(68) Liu, F. C.; Lee, J.; Mayberry, K. A.; Ridgeway, M. E.; Wootton, C. A.; Theisen, A.; Panczyk, E. M.; Jones, B. J.; Nienhaus, L.; Park, M. A.; Bleiholder, C. Direct Observation of Metastable Fragment Ions in Ultraviolet Photodissociation of Ubiquitin. *J. Am. Soc. Mass Spectrom.* **2026**, *37* (4), 910−918.
(69) Crittenden, C. M.; Novelli, E. T.; Mehaffey, M. R.; Xu, G. N.; Giles, D. H.; Fies, W. A.; Dalby, K. N.; Webb, L. J.; Brodbelt, J. S. Structural Evaluation of Protein/Metal Complexes via Native Electrospray Ultraviolet Photodissociation Mass Spectrometry. *J. Am. Soc. Mass Spectrom.* **2020**, *31* (5), 1140−1150.
(70) Horn, D. M.; Ge, Y.; McLafferty, F. W. *Anal. Chem.* **2000**, *72*, 4778−4784.
(71) Hinkle, J. D.; DeFiglia, S. A.; D'Ippolito, R. A.; Mullen, C.; Blakney, G. T.; Yip, P.; Huguet, R.; Hakansson, K.; Shabanowitz, J.; Hunt, D. F.; Syka, J. E. P.; et al. On the Origin of 'Picket Fence' Peaks: Spectral Complexity, Mass Defect Uniformity, and Mass-to-Charge Ratio Alignment in Tandem Mass Spectra of Intact Proteins. *J. Am. Soc. Mass Spectrom*, 2026, accepted.
(72) Kjeldsen, F.; Silivra, O. A.; Ivonin, I. A.; Haselmann, K. F.; Gorshkov, M.; Zubarev, R. A. C $_{\alpha}$ -C Backbone Fragmentation Dominates in Electron Detachment Dissociation of Gas-Phase Polypeptide Polyanions. *Chem. Eur. J.* **2005**, *11* (6), 1803−1812.

Downloaded from pubs.acs.org/jamsef/article-pdf/doi/10.1021/jasms.6c00260/6901816/jasms.6c00260.pdf by FLORIDA STATE UNIV user on 02 November 2026